Performance Analysis of OFDM Systems over 60 GHz Indoor Channels*

Hsin-yueh Hsu†, Tzung-Hua Tsai‡, Wei-De Wu†, and Chi-chao Chao‡
†MediaTek Inc., Hsinchu 30076, Taiwan, R.O.C.
‡Inst. of Communications Engineering, National Tsing Hua University, Hsinchu 30013, Taiwan, R.O.C.
Email: hsinyueh.hsu@mediatek.com, s9964806@m99.nthu.edu.tw, weide.wu@mediatek.com, ccc@ee.nthu.edu.tw

***Abstract*— In this paper, the signal-to-interference-plus-noise ratio (SINR) analysis of orthogonal frequency-division multiplexing (OFDM) systems over the IEEE 802.15.3c 60 GHz channel models is investigated. The derivation precisely captures the distinctive path clustering phenomenon in the spatial-temporal domain and provides the exact SINR. Based on the analytical results, a universal rule for adapting the near-optimal half-power beamwidth is identified. Moreover, numerical results are provided to verify the analytical findings.**

I. Introduction

Owing to the great demand on high-speed wireless communications in short-range environments, 60 GHz communications have attracted considerable interests [1], [2]. IEEE 802.15.3c [3] is one of the important wireless standards operating in the 60 GHz band. The targeted data rate is beyond 1 Gbps, allowing uncompressed high-definition video streaming, very high speed network access, etc.

Due to the very large available bandwidth and the applicability of many compact antennas, 60 GHz channels reveal clusters of random paths in the spatial-temporal domain. In [4], a stochastic channel structure with random path arrivals was utilized to model such phenomenon. The stochastic nature, however, poses certain challenges for theoretical investigation. In fact, most of the performance analyses on 60 GHz systems in the literature were based on simulations over IEEE 802.15.3c channel models [5], [6] or semi-analytical approaches [7], [8]. Analytical results considering the exact channel statistics in the spatial-temporal domain are still lacking.

In this paper, the performance analysis by deriving the exact signal-to-interference-plus-noise ratio (SINR) over IEEE 802.15.3c channel models [4] is provided. The distinctive characteristics of IEEE 802.15.3c channel models in the spatial-temporal domain are precisely captured. In addition, the impact of the antenna directional error due to finite beamforming directions is also included. Based on the novel analytical results, we are able to extensively study the beamforming strategy. It is worth noting that there exists a universal rule for choosing the half-power beamwidth (HPBW) approaching the near-optimal SINR for the case of finite beamforming directions.

*This work was supported by the National Science Council, Taiwan, R.O.C., under Grant NSC 100-2221-E-007-069-MY3.

The organization of the paper is as follows. The channel and system models are introduced in Section II. The SINR analysis is provided in Section III, along with the exact derivation of the channel second-order joint moment. Numerical results are provided in Section IV to verify the analytical findings. Finally, conclusions are drawn in Section V.

II. Channel and System Models

In this section, we give an overview of the IEEE 802.15.3c channel models [4], followed by the system model for 60 GHz orthogonal frequency-division multiplexing (OFDM) systems.

A. IEEE 802.15.3c Channel Models

The IEEE 802.15.3c channel models [4] can be employed to describe the spatial-temporal clustering phenomenon of 60 GHz channels. Specifically, a channel realization is given as

$$h(t,\phi,\theta) = \beta\delta(t)\delta(\phi)\delta(\theta)I_{\text{LOS}} + \sum_{l=1}^{L}\sum_{k\geq 1}\alpha_{k,l}\delta(t-T_l-\tau_{k,l})\delta(\phi-\Psi_l-\psi_{k,l})\delta(\theta-\Theta_l-\omega_{k,l})$$

where β represents the channel gain of the line-of-sight (LOS) path, $\delta(x)$ denotes the Dirac delta function, I_E equals one when the event E is present and zero, otherwise, and L denotes the number of clusters. T_l is the arrival time of the first ray of the l-th cluster, and $\tau_{k,l}$ is the relative delay of the k-th ray of the l-th cluster to T_l. In the spatial domain, Ψ_l and Θ_l are the angle of departure (AOD) and the angle of arrival (AOA) of the first ray of the l-th cluster, respectively, and $\psi_{k,l}$, $\omega_{k,l}$ represent the relative AOD and relative AOA of the k-th ray of the l-th cluster to Ψ_l and Θ_l, respectively. It is noticed that there is no AOD in IEEE 802.15.3c channel models [4]. However, to include the effect of transmitter beamforming, we add the AOD to the channel models with the same distribution as the AOA [7]. The term $\alpha_{k,l}$ denotes the complex amplitude of the k-th ray in the l-th cluster. An example of the channel realization is plotted in Fig. 1.

The number of clusters, L, is assumed to be a random variable with the probability mass function:

$$P_L(l) = \begin{cases} (1+\bar{L})e^{-\bar{L}}, & l=1 \\ \bar{L}^l e^{-\bar{L}}/l!, & l\geq 2 \\ 0, & \text{otherwise} \end{cases}$$

where $\bar{L}$ is the mean of L. The cluster and ray inter-arrival times, i.e., $\{T_l - T_{l-1}\}_{l\geq 2}$ and $\{\tau_{k,l}-\tau_{k-1,l}\}_{k\geq 2}$, are assumed

978-1-4673-1881-5/12/$31.00 ©2012 IEEE

to be independent and identical distributed (i.i.d.) exponential random variables with probability density functions (PDF) $f_c(x) = \Lambda e^{-\Lambda x}$ and $f_r(x) = \lambda e^{-\lambda x}$, respectively. The parameters Λ and λ denote the cluster and ray arrival rates accordingly.

The cluster angles, $\{\Psi_l\}$ and $\{\Theta_l\}$, are i.i.d. uniform random variables distributed over $[0, 2\pi)$. When the LOS path is present, we always set its AOD and AOA to zero as a constant angle rotation does not change the joint distribution of $\{\Psi_l\}$ and $\{\Theta_l\}$. The distributions of the relative AOD's and relative AOA's, $\{\psi_{k,l}\}$ and $\{\omega_{k,l}\}$, are assumed to be independent Laplacian distributions of mean zero and marginal PDF:

$$p(\psi_{k,l}) = \frac{1}{\sqrt{2}\sigma_\psi} \exp\left(-\left|\frac{\sqrt{2}\psi_{k,l}}{\sigma_\psi}\right|\right)$$
$$p(\omega_{k,l}) = \frac{1}{\sqrt{2}\sigma_\omega} \exp\left(-\left|\frac{\sqrt{2}\omega_{k,l}}{\sigma_\omega}\right|\right)$$

where σ_ψ and σ_ω are the standard deviations of $\psi_{k,l}$ and $\omega_{k,l}$, respectively.

The set of complex amplitudes, $\{\alpha_{k,l}\}$, are assumed to have mean zero and second-order moment:

$$E\{\alpha_{k,l}\alpha^*_{k',l'}|T_l, \tau_{k,l}, T_{l'}, \tau_{k',l'}\} = \begin{cases} \Omega_0 e^{-T_l/\Gamma} e^{-\tau_{k,l}/\gamma - \kappa I_{\{k\neq 1\}}} \\ \quad \cdot G(\phi_{3\text{dB}}, \Psi_l + \psi_{k,l} - \hat{\phi}) G(\theta_{3\text{dB}}, \Theta_l + \omega_{k,l} - \hat{\theta}), \\ \qquad \text{if } T_l = T_{l'} \text{ and } \tau_{k,l} = \tau_{k',l'} \\ 0, \qquad \text{otherwise} \end{cases} \quad (1)$$

where Ω_0 is the mean energy at zero channel delay time, Γ and γ denote the cluster and ray decay factors, respectively, κ is the ray Rician factor, and $G(\phi_{3\text{dB}}, \Psi_l + \psi_{k,l} - \hat{\phi})$ and $G(\theta_{3\text{dB}}, \Theta_l + \omega_{k,l} - \hat{\theta})$ are the antenna gains of the transmitter and receiver with HPBW $\phi_{3\text{dB}}$ and $\theta_{3\text{dB}}$, respectively. The antenna gain is modeled by a Gaussian profile representing a realistic beamforming pattern:

$$G(\phi_{3\text{dB}}, \phi - \hat{\phi}) = \frac{4\sqrt{\pi \ln 2}}{\phi_{3\text{dB}}} \exp\left(-\frac{4 \ln 2}{\phi^2_{3\text{dB}}}(\phi - \hat{\phi})^2\right)$$

where $\hat{\phi}$ is the angle corresponding to the maximum gain and is adaptable. An example of the antenna gain profile with $\hat{\phi} = 0$ is plotted in Fig. 2. Note that the value of the HPBW, $\phi_{3\text{dB}}$, is also adaptable. A large HPBW can capture paths from a wide spatial range at the expense of a low beamforming gain at the center angle $\hat{\phi}$. On the other hand, due to feedback limitation, $\hat{\phi}$ and $\hat{\theta}$ are confined to finite directions. We assume that each of $\hat{\phi}$ and $\hat{\theta}$ takes one value from a set of K uniformly separated directions, denoted by $\Phi \triangleq \{2\pi i/K : \lceil \frac{-K+1}{2} \rceil < i \leq \lceil \frac{K-1}{2} \rceil\}$. The selection rule for $\hat{\phi}$ and $\hat{\theta}$ is assumed to be closest to the first arriving path as it possesses the largest path energy on average. Because of the finite resolution, the antenna beam may not exactly point to the first arriving path. Let $\Delta\phi$ denote the directional error. By the angle distribution of the first arriving path, one can check that $\Delta\phi$ is uniformly distributed over $[-\pi/K, \pi/K]$ for non-line-of-sight (NLOS) channels and equals zero for LOS channels.

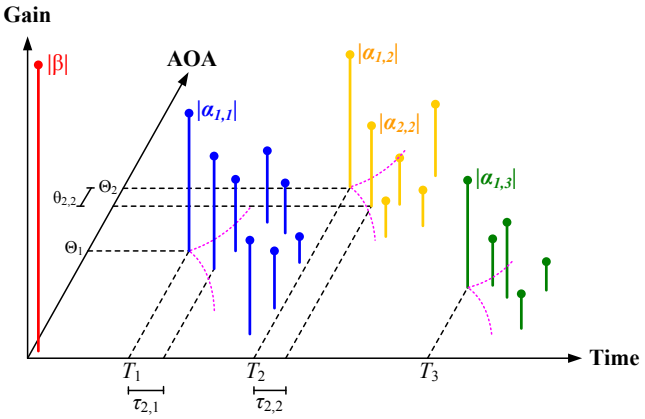

Fig. 1. An example for IEEE 802.15.3c channel models.

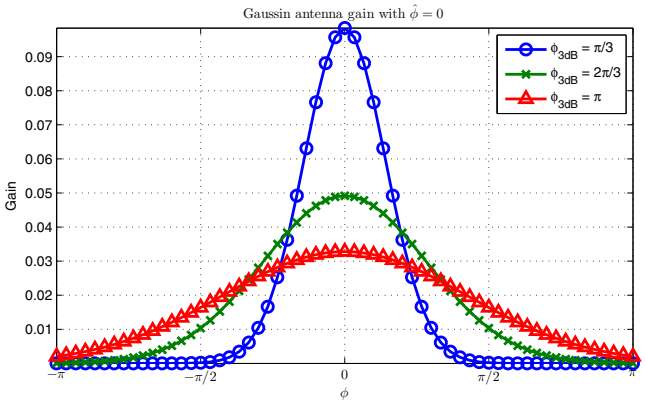

Fig. 2. Gaussian antenna gain.

B. OFDM Systems

By virtue of simple channel equalization and high spectral efficiency, OFDM is a promising candidate for 60 GHz communications. Here we consider an OFDM system with N subcarriers and cyclic prefix length of N_{cp}. Denote $N_s \triangleq N_{cp} + N$ as the time-domain length of an OFDM symbol, and then the time-domain signal can be expressed as

$$x[n] = \sum_{i=-\infty}^{\infty} x_i[n - iN_s].$$

The i-th OFDM symbol multiplexes N frequency-domain data symbols and is given by

$$x_i[n] = w[n] \sum_{k=0}^{N-1} X_{k,i} e^{j\frac{2\pi k(n-N_{cp})}{N}}$$

where $\{X_{k,i}\}$'s denote the data symbols that are uncorrelated of mean zero and energy E_s, and $w[n]$ is the window function which is equal to one for $0 \leq n \leq N_{cp} + N - 1$ and zero, otherwise.

The discrete-time received signal can be obtained as

$$r[n] = \sum_{i=-\infty}^{\infty} \sum_{m=0}^{N-1} h[m] x_i[n - iN_s - m] + \eta[n]$$

where $\{\eta[n]\}$ is the additive white Gaussian noise (AWGN) sample with mean zero and variance N_0, and $\{h[n]\}$ denotes the discrete-time baseband channel impulse response with

$$h[n] \triangleq \int_{-\infty}^{\infty}\int_{-\pi}^{\pi}\int_{-\pi}^{\pi} g(nT-t)h(t,\phi,\theta)d\phi d\theta dt$$
$$= \beta g(nT)I_{\text{LOS}} + \sum_{l=1}^{L}\sum_{k\geq 1}\alpha_{k,l}g(nT-T_l-\tau_{k,l}) \quad (2)$$

where T denotes the sampling interval and $g(t)$ represents the pulse-shaping function. To have the unit pulse energy, we set $g(0)=1$.

After the discrete Fourier transform is performed on $r[n]$, the received signal on the k-th subcarrier of the i-th OFDM symbol can be given by

$$R_i[k] = H[k]X_{k,i} + Z_{k,i}^{\text{ICI}} + Z_{k,i}^{\text{ISI}} + V_{k,i}$$

where $H[k] \triangleq \sum_{n=0}^{N-1} h[n]e^{-j\frac{2\pi nk}{N}}$ is the frequency-domain channel response on the k-th subcarrier, $Z_{k,i}^{\text{ICI}}$ denotes the inter-carrier interference (ICI) from other subcarriers, $Z_{k,i}^{\text{ISI}}$ represents the inter-symbol interference (ISI) from previous OFDM symbols, and $V_{k,i}$ denotes the k-th frequency domain noise component. Furthermore, we can have

$$Z_{k,i}^{\text{ICI}} = \frac{1}{N}\sum_{m,n=0}^{N-1} h[m]x_i[n-m+N_{cp}]e^{-j\frac{2\pi nk}{N}} - H[k]X_{k,i} \quad (3)$$

$$Z_{k,i}^{\text{ISI}} = \frac{1}{N}\sum_{i'<i}\sum_{m,n=0}^{N-1} h[m]x_{i'}[n-m+(i-i')N_s+N_{cp}]e^{-j\frac{2\pi nk}{N}} \quad (4)$$

$$V_{k,i} = \frac{1}{N}\sum_{n=0}^{N-1}\eta[n+iN_s+N_{cp}]e^{-j\frac{2\pi nk}{N}} \quad (5)$$

and the above will be utilized in the following performance analysis.

III. Exact Performance Analysis

A. Signal-to-Interference-Plus-Noise Ratio

In this section, we analyze the performance by deriving the exact SINR. The SINR for the k-th subcarrier is defined as

$$\text{SINR}_k \triangleq \frac{E\{|H[k]X_{k,i}|^2\}}{E\{|R_i[k]-H[k]X_{k,i}|^2\}} = \frac{E_sE\{|H[k]|^2\}}{E\{|Z_{k,i}^{\text{ICI}}|^2\}+E\{|Z_{k,i}^{\text{ISI}}|^2\}+E\{|V_{k,i}|^2\}}. \quad (6)$$

By expanding $E\{|H[k]|^2\}$, $E\{|Z_{k,i}^{\text{ICI}}|^2\}$, $E\{|Z_{k,i}^{\text{ISI}}|^2\}$, $E\{|V_{k,i}|^2\}$, with (3), (4), and (5), one can obtain

$$E\left\{|H[k]|^2\right\} = \sum_{n,n'=0}^{N-1}\mathcal{H}[n,n']e^{-j\frac{2\pi(n-n')k}{N}} \quad (7)$$

$$E\left\{|Z_{k,i}^{\text{ISI}}|^2\right\} = \frac{1}{N^2}\sum_{i'<i}\sum_{k',n,n',m,m'=0}^{N-1} w[m-n+(i-i')N_s+N_{cp}]w[m'-n'+(i-i')N_s+N_{cp}]\mathcal{H}[n,n']E\{|X_{k',i}|^2\}e^{-j\frac{2\pi(n-n')k'}{N}}e^{-j\frac{2\pi(m-m')(k-k')}{N}} \quad (8)$$

$$E\left\{|Z_{k,i}^{\text{ICI}}|^2\right\} = E_s\sum_{n,n'=0}^{N-1}\mathcal{H}[n,n']e^{-j\frac{2\pi(n-n')k}{N}} + \frac{1}{N^2}\sum_{k',n,n',m,m'=0}^{N-1} w[m-n+N_{cp}]w[m'-n'+N_{cp}]E\{|X_{k',i}|^2\}\cdot\mathcal{H}[n,n']e^{-j\frac{2\pi(n-n')k'}{N}}e^{-j\frac{2\pi(m-m')(k-k')}{N}} - 2\text{Re}\left\{\frac{E_s}{N}\sum_{m,n,n'=0}^{N-1} w[m-n+N_{cp}]\mathcal{H}[n,n']e^{-j\frac{2\pi(n-n')k}{N}}\right\} \quad (9)$$

$$E\{|V_{k,i}|^2\} = N_0/N \quad (10)$$

where $\text{Re}\{x[n]\}$ represents the real part of $x[n]$ and $\mathcal{H}[n,n'] \triangleq E\{h[n]h^*[n']\}$ is the channel second-order joint moment. To obtain the exact SINR, we need to derive the channel second-order joint moment regarding both the spatial and temporal statistics of the random arriving paths.

B. Exact Channel Second-Order Joint Moment

For the exact channel second-order joint moment for IEEE 802.15.3c channels, we first expand $\mathcal{H}[n,n']$ with (1) and (2) and obtain

$$\mathcal{H}[n,n'] = \beta^2 g(nT)g(n'T)I_{\text{LOS}} + E_{\text{D}}\left\{\sum_{l=1}^{L}\sum_{k\geq 1}\Omega_0 e^{-T_l/\Gamma}e^{-\tau_{k,l}/\gamma-\kappa I_{\{k\neq 1\}}}\cdot g(nT-T_l-\tau_{k,l})g(n'T-T_l-\tau_{k,l})\right\}\cdot E_{\text{A}}\left\{G(\phi_{3\text{dB}},\Psi_l+\psi_{k,l}-\hat{\phi})\right\}E_{\text{A}}\left\{G(\theta_{3\text{dB}},\Theta_l+\theta_{k,l}-\hat{\theta})\right\}$$

where $E_{\text{D}}\{\cdot\}$ and $E_{\text{A}}\{\cdot\}$ denote the averages over the random path delays and random path angles, respectively. By the assumption that $\hat{\phi}$ and $\hat{\theta}$ are chosen closest to the angle of the first arriving path, one can have

$$G(\phi_{3\text{dB}},\Psi_l+\psi_{k,l}-\hat{\phi}) = \begin{cases} G(\phi_{3\text{dB}},\Psi_l+\psi_{k,l}), & \text{for LOS channels} \\ G(\phi_{3\text{dB}},\Psi_l-\Psi_1+\psi_{k,l}-\Delta\phi), & \text{for NLOS channels.}\end{cases}$$

For LOS channels, we can further classify the paths into two groups. One comprises the first rays of all clusters and the other group includes all other paths. The first group only depends on Ψ_l and the other depends on both Ψ_l and $\psi_{k,l}$. For NLOS channels, the average of $G(\phi_{3\text{dB}},\Psi_l-\Psi_1+\psi_{k,l}-\Delta\phi)$ depends on $\Psi_l-\Psi_1$, $\psi_{k,l}$, and $\Delta\phi$, and we will classify the paths into four groups. The first contains the first ray within the first cluster whose antenna gain only depends on $\Delta\phi$. The second group comprises the other rays in the first cluster whose antenna gains depend on $\psi_{k,l}$ and $\Delta\phi$. The third group includes the first rays of all non-first clusters whose antenna gains depend on $\Psi_l-\Psi_1$ and $\Delta\phi$, and the fourth group embraces all other paths whose antenna gains depend on $\Psi_l-\Psi_1$, $\psi_{k,l}$, and $\Delta\phi$.

Denote $\tilde{A}_{i,t}$ and $\tilde{A}_{i,r}$ as the average effects of transmitter and receiver antenna gains for a path belonging to the i-th group, respectively. Then, one can have, for LOS channels,

$$\tilde{A}_{1,t} = \tilde{A}_{2,t} = 1 - 2Q(\pi\sqrt{2\alpha})$$

where $Q(x) \triangleq (2\pi)^{-\frac{1}{2}} \int_x^\infty \exp(-u^2/2)du$ and $\alpha = 4\ln 2/\phi_{3\text{dB}}^2$. For NLOS channels, it can be checked that

$$\begin{aligned}
\tilde{A}_{1,t} &= K\left[1 - 2Q(\pi\sqrt{2\alpha}/K)\right] \\
\tilde{A}_{2,t} &= \frac{K}{(1-p)}\left\{1 - 2Q\left(\pi\sqrt{2\alpha}/K\right)\right. \\
&\quad + 2e^{-\frac{\pi\sqrt{2}}{\sigma_\psi}}\left[Q\left(\pi\sqrt{2\alpha}\right) - Q\left(\pi\sqrt{2\alpha}\,(1-1/K)\right)\right] \\
&\quad + e^{\frac{\pi\sqrt{2}}{K\sigma_\psi} + \frac{1}{2\sigma_\psi^2\alpha}}\left[Q\left(\sqrt{2\alpha}\left((2\sigma_\psi^2\alpha)^{-1} + \pi/K\right)\right)\right. \\
&\qquad \left. - Q\left(\sqrt{2\alpha}\left((2\sigma_\psi^2\alpha)^{-1} + \pi\right)\right)\right] \\
&\quad - e^{-\frac{\pi\sqrt{2}}{K\sigma_\psi} + \frac{1}{2\sigma_\psi^2\alpha}}\left[Q\left(\sqrt{2\alpha}\left((2\sigma_\psi^2\alpha)^{-1} - \pi/K\right)\right)\right. \\
&\qquad \left. - Q\left(\sqrt{2\alpha}\left((2\sigma_\psi^2\alpha)^{-1} + \pi(1-1/K)\right)\right)\right] \\
&\quad + e^{-\frac{\pi\sqrt{2}}{\sigma_\psi}\left(2-\frac{1}{K}\right) + \frac{1}{2\sigma_\psi^2\alpha}}\left[Q\left(\sqrt{2\alpha}\left(\pi(1-1/K) - (2\sigma_\psi^2\alpha)^{-1}\right)\right)\right. \\
&\qquad \left.\left. - Q\left(\sqrt{2\alpha}\left(\pi - (2\sigma_\psi^2\alpha)^{-1}\right)\right)\right]\right\} \\
\tilde{A}_{3,t} &= \tilde{A}_{4,t} = 1 - 2Q(\pi\sqrt{2\alpha})
\end{aligned}$$

where $p = \exp(-\pi\sqrt{2}/\sigma_\psi)$. Note that the receiver counterparts, $\{\tilde{A}_{i,r}\}_{i=1}^4$, can be obtained by replacing σ_ψ and $\phi_{3\text{dB}}$ by σ_ω and $\theta_{3\text{dB}}$, respectively.

To derive the exact channel second-order joint moment, one needs to utilize the extended density functions in [9] that are used to represent the average effect of time-domain random arrivals. After some lengthy calculation for each path group (skipped here due to space limitation), we can obtain, for NLOS channels,

$$\mathcal{H}[n,n'] = \int_0^\infty g(nT-t)g(n'T-t)q_2(t)dt \qquad (11)$$

where

$$\begin{aligned}
&q_2(t) \\
&= \Omega_0\left\{\Lambda\left[\tilde{A}_{3,t}\tilde{A}_{3,r}e^{-t/\Gamma} + \left(\tilde{A}_{1,t}\tilde{A}_{1,r} - \tilde{A}_{3,t}\tilde{A}_{3,r}\right)e^{-t(\Lambda+1/\Gamma)}\right]\right. \\
&\quad - \sum_{i=1}^\infty E_i(\bar{L})G_{i+1}(t)e^{-t/\Gamma}\tilde{A}_{3,t}\tilde{A}_{3,r} \\
&\quad + \lambda e^{-\kappa}\left[\Lambda\epsilon\left(e^{-t/\gamma} - e^{-t(\Lambda+1/\Gamma)}\right)\left(\tilde{A}_{2,t}\tilde{A}_{2,r} - \tilde{A}_{4,t}\tilde{A}_{4,r}\right)\right. \\
&\left.\left. + \Lambda\rho\tilde{A}_{4,t}\tilde{A}_{4,r}\left(e^{-t/\gamma} - e^{-t/\Gamma}\right) - \tilde{A}_{4,t}\tilde{A}_{4,r}\sum_{i=1}^\infty E_i(\bar{L})B_i(t)e^{-t/\gamma}\right]\right\}
\end{aligned}$$

with

$$E_i(\bar{L}) \triangleq e^{-\bar{L}}\sum_{l=0}^i \frac{\bar{L}^l}{l!}, \qquad G_{i+1}(t) \triangleq \frac{e^{-\Lambda t}\Lambda^{i+1}t^i}{i!}$$

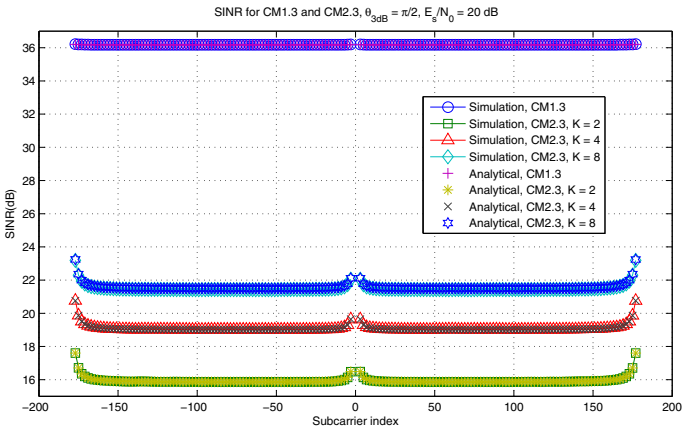

Fig. 3. SINR for CM1.3 and CM2.3, $\theta_{3\text{dB}} = \pi/2$, $E_s/N_0 = 20$ dB.

$$B_i(t) \triangleq (\Lambda\epsilon)^{i+1}\left(1 - \sum_{l=0}^i \frac{e^{-t/\epsilon}(t/\epsilon)^l}{l!}\right)$$

$$\rho \triangleq \frac{1}{\frac{1}{\Gamma} - \frac{1}{\gamma}}, \qquad \epsilon \triangleq \frac{1}{\Lambda + \frac{1}{\rho}}.$$

For LOS channels, one can have

$$\begin{aligned}
&\mathcal{H}[n,n'] \\
&= \beta^2 g(nT)g(n'T) + \int_0^\infty g(nT-t)g(n'T-t)q_2'(t)dt \qquad (12)
\end{aligned}$$

where

$$\begin{aligned}
q_2'(t) &= \Omega_0\left\{\tilde{A}_{1,t}\tilde{A}_{1,r}e^{-t/\Gamma}\left[\Lambda - \sum_{i=1}^\infty E_i(\bar{L})G_{i+1}(t)\right]\right. \\
&\left. + \tilde{A}_{2,t}\tilde{A}_{2,r}\lambda e^{-\kappa}\left[\Lambda\rho\left(e^{-t/\gamma} - e^{-t/\Gamma}\right) - \sum_{i=1}^\infty E_i(\bar{L})B_i(t;\epsilon)e^{-t/\gamma}\right]\right\}.
\end{aligned}$$

With the above results, the exact SINR can now be computed by (6)–(12).

IV. Numerical and Simulation Results

In this section, the exactness of the derived analytical SINR will be verified by simulations. A universal rule for choosing the near-optimal HPBW will also be identified through evaluating the SINR. The pulse-shaping function $g(t)$ is assumed to be the raised cosine function with roll-off factor 0.3. The HPBW of the transmitter antenna and the subcarrier allocation follow the IEEE 802.15.3c specification [3]. Since signals in indoor environments are usually strong, we set E_s/N_0 to be 20 dB. We will show our results over CM1.3 and CM2.3 corresponding to LOS and NLOS residential environments [4], respectively. Note that we only present the SINR results as systems usually have similar performance trends in optimizing SINR and bit error rate [10].

In Fig. 3, the analytical SINRs for $K = 2, 4$, and 8 where K is the number of available antenna directions are compared with simulation results. We only present one curve for LOS channels since the analytical result is independent of K. It can be checked that the simulation results well match the analytical results in all cases. Due to the ICI effect, the SINR values

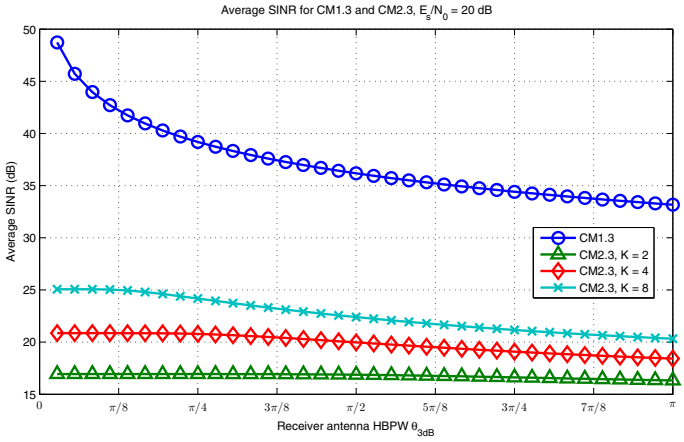

Fig. 4. Average SINR for CM1.3 and CM2.3, $E_s/N_0 = 20$ dB.

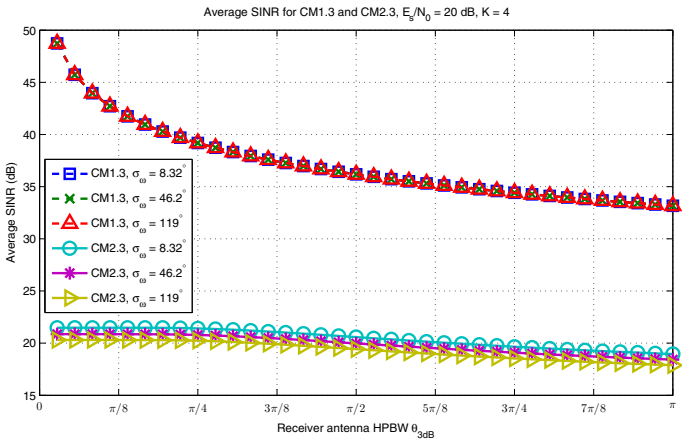

Fig. 5. Average SINR for CM1.3 and CM2.3, $E_s/N_0 = 20$ dB, $K = 4$.

for subcarrier index ranging from -160 to -15 and from 15 to 160 are smaller than others. The LOS channel has better performance than NLOS channels. Also the performance for NLOS channels improves when K increases, which is because increasing K reduces the directional error and improves the effect of beamforming. For the LOS channel, there is no such difference because of no directional error in our setting.

In Fig. 4, the average SINR over the whole frequency band versus different values of the HPBW is shown, where the average SINR is defined as

$$\text{SINR} \triangleq \frac{\sum_{k\in\mathcal{D}} E\{|H[k]X_{k,i}|^2\}}{\sum_{k\in\mathcal{D}} E\{|R_i[k] - H[k]X_{k,i}|^2\}}$$

and $\mathcal{D}$ denotes the index set of data subcarriers. One can see that the average SINR improves when the receiver antenna HPBW decreases, corresponding to more concentrated beamforming. However, the improvement for NLOS channels vanishes when the HPBW becomes smaller than π/K. Therefore, one may conclude a universal rule for NLOS channels that setting HPBW to π/K for any given value of K is sufficient to approach the optimal SINR. On the other hand, regarding the constant LOS path in LOS channels, setting a smaller HPBW can multiply the LOS energy with a larger beamforming gain, thereby showing non-vanishing SINR improvement along with small HPBW.

In Fig. 5, the average SINR versus receiver antenna HPBW under different values of the channel spatial spread parameter σ_ω is shown. For NLOS channels, because the probability that the rays fall outside a given beamforming coverage is increasing for increasing σ_ω, the average SINR degrades accordingly. On the other hand, since the SINR is dominated by the LOS path in LOS channels, the change of σ_ω does not affect the performance. Yet, the SINR for NLOS channels still approaches the optimal one when the HPBW is set to π/K. This also strengthens the applicability of the proposed universal rule in different channel conditions.

V. Conclusion

In this paper, the exact SINR analysis of OFDM systems over IEEE 802.15.3c channel models is performed. The distinctive path clustering phenomenon in the spatial-temporal domain is precisely captured in our analysis. The accuracy of the analytical results is verified by numerical simulations. A universal rule that is useful for choosing a near-optimal HPBW is also identified.

Our current analysis assumes one single directional beamforming pattern that may not adequately exploit the rich spatial-temporal path diversity in 60 GHz channels. A possible future work is to extend our analysis to multi-directional beamforming or more advanced beamforming codebooks for 60 GHz communications.

References

[1] R. C. Daniels and R. W. Heath, "60 GHz wireless communications: Emerging requirements and design recommendations," *IEEE Veh. Technol. Mag.*, vol. 2, no. 3, pp. 41–50, Sep. 2007.

[2] S.-K. Yong and C.-C. Chong, "An overview of multigigabit wireless through millimeter wave technology: Potentials and technical challenges," *EURASIP J. Wireless Commun. and Networking*, vol. 2007, no. 1, pp. 50–50, Jan. 2007.

[3] "IEEE standard for information technology - Telecommunications and information exchange between systems - Local and metropolitan area networks - Specific requirements. Part 15.3: Wireless medium access control (MAC) and physical layer (PHY) specifications for high rate wireless personal area networks (WPANs) amendment 2: Millimeter-wave-based alternative physical layer extension," *IEEE Std 802.15.3c-2009 (Amendment to IEEE Std 802.15.3-2003)*, pp. c1–187, Oct. 2009.

[4] S.-K. Yong, et al., "TG3c channel modeling sub-committee final report," *IEEE doc.:IEEE 802.15-07-0584-01-003c*, Sep. 2010.

[5] C. Yiu and S. Singh, "Empirical capacity of mmWave WLANs," *IEEE J. Sel. Areas Commun.*, vol. 27, no. 8, pp. 1479–1487, Oct. 2009.

[6] X. Zhu, A. Doufexi, and T. Kocak, "On the performance of IEEE 802.15.3c millimeter-wave WPANs: PHY and MAC," in *Proc. 6th Conf. Wireless Advanced*, London, UK, Jun. 2010, pp. 1–6.

[7] S. Yoon, T. Jeon, and W. Lee, "Hybrid beam-forming and beam-switching for OFDM based wireless personal area networks," *IEEE J. Sel. Areas Commun.*, vol. 27, no. 8, pp. 1425–1432, Oct. 2009.

[8] T. V. Nguyen, E. Masry, and L. B. Milstein, "Channel model and performance analysis of QAM multiple antenna systems at 60-GHz in the presence of human activity," in *Proc. IEEE Global Commun. Conf.*, Houston, TX, Dec. 2011, pp. 1–6.

[9] J.-Y. Chang, W.-D. Wu, and C.-C. Chao, "An analytical framework for ultra-wideband communications over IEEE 802.15.4a channels," in *Proc. IEEE Int. Symp. Inform. Theory*, Toronto, Canada, Jul. 2008, pp. 2757–2761.

[10] T. Jia and D. I. Kim, "Analysis of channel-averaged SINR for indoor UWB Rake and transmitted reference systems," *IEEE Trans. Commun.*, vol. 55, no. 10, pp. 2022–2032, Oct. 2007.